Earth and Planetary Science Letters 285 (2009) 263–271

Contents lists available at ScienceDirect

Earth and Planetary Science Letters

journal homepage: www.elsevier.com/locate/epsl

Explosive volcanic eruptions on Mercury: Eruption conditions, magma volatile content, and implications for interior volatile abundances

Laura Kerber [a,*], James W. Head [a], Sean C. Solomon [b], Scott L. Murchie [c], David T. Blewett [c], Lionel Wilson [d]

[a] Geological Sciences Department, Brown University, 324 Brook Street, Box 1846, Providence, RI 02912, USA
[b] Department of Terrestrial Magnetism, Carnegie Institution of Washington, 5241 Broad Branch Road, N.W., Washington, DC 20015, USA
[c] The Johns Hopkins University Applied Physics Laboratory, 11100 Johns Hopkins Road, Laurel, MD 20723, USA
[d] Environmental Science Department, Lancaster University, Lancaster LA1 4YQ, UK

ARTICLE INFO

Article history:
Accepted 27 April 2009
Available online 29 May 2009

Editor: T. Spohn

Keywords:
Mercury
pyroclastic
volcanism
volatile
accretion
interior
MESSENGER

ABSTRACT

Images obtained by the MESSENGER spacecraft have revealed evidence for pyroclastic volcanism on Mercury. Because of the importance of this inference for understanding the interior volatile inventory of Mercury, we focus on one of the best examples determined to date: a shield-volcano-like feature just inside the southwestern rim of the Caloris impact basin characterized by a near-central, irregularly shaped depression surrounded by a bright deposit interpreted to have a pyroclastic origin. This candidate pyroclastic deposit has a mean radius of ~24 km, greater in size than the third largest lunar pyroclastic deposit when scaled to lunar gravity conditions. From the extent of the candidate pyroclastic deposit, we characterize the eruption parameters of the event that emplaced it, including vent speed and candidate volatile content. The minimum vent speed is ~300 m/s, and the volatile content required to emplace the pyroclasts to this distance is hundreds to several thousands of parts per million (ppm) of the volatiles typically associated with pyroclastic eruptions on other bodies (e.g., CO, CO_2, H_2O, SO_2, H_2S). For comparison, measurements of the exsolution of volatiles (H_2O, CO_2, S) from basaltic eruptive episodes at Kilauea volcano, Hawaii, indicate values of ~1300–6500 ppm for the terrestrial mantle source. Evidence for the presence of significant amounts of volatiles in partial melts derived from the interior of Mercury is an unexpected result and provides a new constraint on models for the planet's formation and early evolution.

© 2009 Elsevier B.V. All rights reserved.

1. Introduction

The planet Mercury is generally thought to be deficient in interior volatiles compared with the other terrestrial planets (e.g., Boynton et al., 2007). Numerical simulations of planetary accretion indicate that Mercury is likely to be dominated by material formed in the inner solar nebula (Wetherill, 1994), where temperatures were comparatively high and volatile species remained in the gas phase throughout the time interval when nebular gas was present (e.g., Boss, 1998; Chambers, 2005). Several of the scenarios proposed to account for Mercury's anomalously high bulk density (and inferred high ratio of metal to silicate) involve one or more episodes of further heating, either by the nebula itself (Cameron, 1985; Fegley and Cameron, 1987) or as a result of collision with another large object (Wetherill, 1988; Benz et al., 1988, 2007). Such heating should further deplete volatile species in Mercury's interior (Boynton et al., 2007). Moderately volatile alkali metals are known to be important surface-derived species in Mercury's exosphere (Potter and Morgan, 1985, 1986), and polar deposits postulated to consist of water ice have been documented by Earth-based radar on the floors of permanently shadowed impact craters near Mercury's poles (Harmon and Slade, 1992; Slade et al., 1992); these volatiles may be derived dominantly from meteoritic and cometary sources (e.g., Moses et al., 1999; Leblanc and Johnson, 2003), however, and need not constrain interior volatile abundances.

An important new constraint on interior volatile abundances on Mercury comes from imaging conducted during the first flyby of Mercury by the MErcury Surface, Space ENvironment, GEochemistry, and Ranging (MESSENGER) spacecraft (Solomon et al., 2008). MESSENGER images of the 1550-km-diameter Caloris basin reveal several irregular depressions surrounded by bright, relatively red deposits (compared to Mercury as a whole). Detailed assessment of morphologic characteristics indicates that these features are broad, low shield volcanoes (Head et al., 2008, 2009a-this issue). By analogy with similar features on the Moon, the haloes of diffuse-bordered, high-reflectance material surrounding several of these irregular depressions are interpreted as pyroclastic deposits (Head et al., 2008, 2009a-this issue), which are the product of explosive volcanic eruptions driven by the exsolution of magmatic volatiles during ascent of the magma from the mantle or lower crust (e.g., Wilson and Head, 1981). These volcanic features therefore provide evidence for volatiles in Mercury's mantle or lower crust at the time of magma genesis.

In this paper we offer a detailed rationale for the identification of pyroclastic deposits on Mercury, some inferences on eruption

* Corresponding author. Tel.: +1 401 863 3841; fax: +1 401 863 3978.
E-mail address: Laura_Kerber@brown.edu (L. Kerber).

0012-821X/$ – see front matter © 2009 Elsevier B.V. All rights reserved.
doi:10.1016/j.epsl.2009.04.037

conditions and magmatic volatile contents consistent with the geometry of observed deposits, and an assessment of the implications of these findings for the volatile budget of Mercury's interior. We begin with a summary of what is known of pyroclastic deposits on the Moon as a basis for comparison with features on Mercury; we pay particular attention to possible causes for spectral and albedo differences between pyroclastic deposits on the Moon and Mercury. We then provide a detailed examination of a type example of pyroclastic deposits on Mercury. We derive estimates of the eruption velocity and the volatile content of the magma consistent with such estimates for candidate volatile species. We summarize constraints on Mercury's formation history and volatile inventory, and we discuss how the identification of pyroclastic eruption conditions on Mercury provides new constraints on these issues.

2. Characteristics of pyroclastic deposits on the Moon

Local and regional deposits interpreted to be of pyroclastic origin have long been recognized on the Moon (Wilhelms and McCauley, 1971; Scott et al., 1977), generally in association with irregular depressions, sinuous rilles, or fractures in large crater floors (Head, 1974; Lucchitta and Schmitt, 1974; Wilson and Head, 1981; Gaddis et al., 1985; Hawke et al., 1989; Weitz et al., 1998; Weitz and Head, 1999; Gaddis et al., 2003). Regional deposits are the most areally extensive (areas greater than 1000 km^2) and are commonly located on uplands adjacent to younger mare deposits (e.g., Head, 1974; Weitz et al., 1998). Localized deposits, in contrast, are smaller in extent and more widely distributed across the lunar surface (Head, 1976; Hawke et al., 1989; Coombs et al., 1990). The albedo of lunar pyroclasts is generally low, although some deposits have a slightly higher albedo (perhaps due to intermixed mature lunar highlands material), such as those at J. Herschel and Orientale (Gaddis et al., 2003). Indeed, the low albedo of lunar pyroclastic deposits has long been part of their definition, and the deposits are often called lunar dark mantle deposits or material (Pieters et al., 1974; Weitz et al., 1998).

Surface geological exploration at the Apollo landing sites and multispectral telescopic observations of the dark mantle deposits indicate that they are composed of submillimeter volcanic glasses or crystallized beads. The reflectance spectra of the lunar pyroclastic deposits are influenced by their style of emplacement and cooling, chemical composition, grain size distribution, and age. For example, the Taurus–Littrow deposit spectrally matches the crystallized black beads that were collected at the Apollo 17 landing site (Pieters et al., 1974), whereas the Aristarchus Plateau deposit is dominated by orange and red glasses (Zisk et al., 1977; Lucey et al., 1986). Remote-sensing data for numerous more localized deposits (Hawke et al., 1989) show evidence for three compositional groups, each reflecting variation in the eruption conditions associated with their emplacement. The effects of various eruption conditions are discussed in detail in the next section.

Depending on their chemical compositions, lunar volcanic glasses may have a variety of colors, including clear, red, orange, brown, yellow, and green (Delano, 1986). Absorptions at optical wavelengths are dependent on electronic transitions associated with ferrous iron in silicates, which generally lowers the reflectance due to overlapping ultraviolet (UV) and near-infrared (NIR) bands and produces an absorption feature at wavelengths near 1 μm (e.g., Burns 1993; Lucey et al., 1998). The combined presence of Fe and Ti can lower the albedo due to Fe–Ti charge-transfer bands, while low-Ti glasses, such as the Apollo 15 green glasses, do not have low reflectances at visible wavelengths (Bell et al., 1976; Wells and Hapke, 1977; Lucey et al., 1998). Orange glasses tend to have a steeper (or "redder") spectral slope at visible and NIR wavelengths because they have an abundance of TiO_2 (Gaddis et al., 2003). In contrast, the titanium in black pyroclastic beads is incorporated during crystallization into the mineral ilmenite ($FeTiO_3$), which crystallizes inside the glass as laths and gives black beads a low-reflectance, more shallowly sloping (or "bluer") spectrum that closely resembles that of bulk ilmenite (Pieters et al., 1974; Weitz et al., 1998).

Many lunar pyroclastic samples contain large amounts of FeO (16.5 to 24.7 wt.%) (Delano, 1986). However, the surface of Mercury appears to be depleted in silicates containing ferrous iron because reflectance spectra largely lack the distinctive absorption feature near 1 μm (e.g., Vilas, 1988; Warell, 2003; Warell and Blewett, 2004; Warell et al., 2006; McClintock et al., 2008; Robinson et al., 2008). Despite the dearth of ferrous iron in silicates, Mercury's surface nonetheless darkens and reddens with time like that of the Moon. This darkening and reddening has been interpreted to be the result of production of nanophase iron (e.g., Pieters et al., 2000; Hapke, 2001), which could be derived from an opaque phase in the crustal material or from delivery by micrometeorite impacts (Noble and Pieters, 2003). On the Moon, deposits that are brighter and redder than the average Moon spectrum appear to be lower in iron (e.g., highland material); deposits that are darker and redder than average are higher in iron (e.g., low-Ti mare material) (Lucey et al., 1995). Crater ray materials on Mercury are brighter and bluer than the general Mercury spectrum, indicating that they are younger, and thus not yet as space weathered. The enigmatic "bright crater floor deposits" (Robinson et al., 2008) are also bright but with an even bluer relative spectrum. Deposits that are darker and bluer than average for Mercury are interpreted to be higher in opaque minerals (potentially ilmenite) than other units (Robinson et al., 2008; Blewett et al., 2009-this issue). By analogy, pyroclasts on Mercury would be expected to be brighter and redder than surrounding units if they had less ferrous iron, titanium, and opaque minerals, or darker and bluer than surrounding units if the magma were relatively opaque-rich (or if some Fe and Ti were available). If the nanophase iron produced during space weathering is derived from iron-bearing phases on the surface, pyroclastic deposits with lower iron content and few iron-bearing opaque minerals would darken less during space weathering than more iron-rich deposits and thus remain brighter over time. If the iron is delivered to the surface by micrometeoroid bombardment, the deposit would be expected to darken at rates similar to other deposits.

Decreasing grain size generally increases visible reflectance. The properties of the magma source and the proportion of volatiles present in a pyroclastic eruption can influence the grain size of the deposit (Wilson and Head, 1981), as discussed below.

3. Formation of pyroclastic deposits

Pyroclastic eruptions take place when volatile species in rising magma exsolve at reduced pressure. Enough energy must be available both to convert the volatile phase to a gas and to overcome the viscosity of the host liquid and allow gas bubbles to grow. Depending on the characteristics of the magma, the nucleation of many bubbles can be favored or, alternatively, the continued growth of several large bubbles may occur. Bubbles nucleate and grow as the magma rises until they reach the point at which the bubble walls cease to deform plastically and shatter, resulting in fragmentation and ejection from the vent (Wilson and Head, 1981). The thin walls of the bubbles and the inter-bubble liquid become the resulting pyroclasts. The size of the pyroclasts is thus related to the bubble size, which is controlled by several parameters, including the volatile content of the magma, the magma viscosity, and its temperature (Wilson and Head, 1981). Roughness and irregularities in the vent can also contribute to the nucleation of bubbles, because pockets of roughness create sporadic zones with slightly less pressure, allowing bubbles to nucleate at somewhat lower temperatures or greater depths. The difference in spectral characteristics expected on Mercury as a result of grain size is thus difficult to predict.

Spectral and morphological differences among pyroclastic deposits may also be due in part to different eruption styles, which lead to

varied cooling histories (Head and Wilson, 1979; Wilson and Head, 1981). In Hawaiian-style eruptions, the rise speed of the magma is fairly constant, and exsolved volatiles contribute to a steadily erupting fountain that disperses pyroclastic beads (Wilson and Head, 1981). In Vulcanian-style eruptions, the exsolved gases build up below a strong plug or cap rock until the pressure causes failure of the plug, resulting in a short, violent eruption that disperses disrupted magma as pyroclasts as well as fractured plug material and country rock (Head and Wilson, 1979). In Strombolian-style eruptions, the gas exsolution rate exceeds the rise rate of the magma, and bubble coalescence causes large gas bubbles to break through and disrupt the lava surface sporadically, emplacing bursts of pyroclastic beads (Head and Wilson, 1979). Depending on which type of eruption occurs, the admixture of pyroclasts, magma-derived basaltic material, and country rock may vary. For example, a lunar Vulcanian eruption could yield pyroclasts, shards of basaltic plug rock, and pieces of anorthositic country rock. For eruptions that take place in the lunar maria, the country rock is basaltic, resulting in a comparatively higher proportion of basalt and a lower albedo (Head and Wilson, 1989). For Hawaiian-style fountain eruptions, pyroclastic quenched glasses and beads may dominate the spectra (Head and Wilson, 1989). As on the Earth and the Moon, any of these types of eruptions may theoretically take place on Mercury, leading to some variety in the expected deposits.

On the basis of the context given above, we focus on a particular pyroclastic deposit discovered on the hemisphere newly imaged by the MESSENGER spacecraft during its first Mercury flyby. We examine the deposit's spectrum and dimensions in order to gain information related to the magmatic volatile content and the interior volatile budget of Mercury.

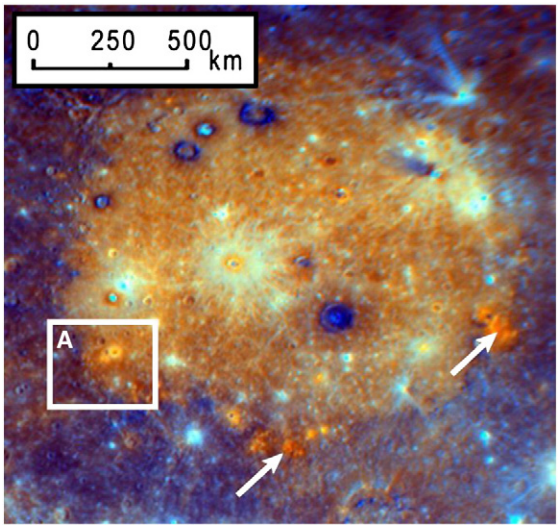

Fig. 1. Principal component (PC) color-composite image of the Caloris basin interior and margins at 5 km/pixel spatial resolution derived from multispectral WAC image mosaics (Murchie et al., 2008; Robinson et al., 2008). Red = PC2, green = PC1, blue = 430-nm/1000-nm ratio. PC1 is sensitive to compositional variations related to the abundance of opaque phases (brighter = lower opaque content). PC2 mainly records variations in regolith maturity (brighter = less mature). Box A shows the area of interest and the extent of Fig. 2. Features with anomalous color, interpreted as pyroclastic deposits, appear as orange pixels and are located around the southern rim of the Caloris basin (arrows).

4. Pyroclastic deposits on Mercury

On Mercury, several possible pyroclastic deposits were identified from Mariner 10 data. They show diffuse boundaries and draping rather than embayment relationships (Rava and Hapke, 1987; Robinson and Lucey, 1997). Rava and Hapke (1987) suggested that diffuse, high-reflectance material with relatively red color on the floor of Lermontov could be pyroclastic in origin (see also Blewett et al., 2007). Robinson and Lucey (1997) identified two potential pyroclastic deposits in their reprocessed Mariner 10 spectral parameter images. The relatively low albedo, high opaque index, and blue spectrum of these deposits are consistent with a mafic composition similar to the composition of lunar pyroclastic deposits (Robinson and Lucey, 1997). One deposit appears to be associated with a linear feature on the rim of the Homer basin, and then second is northwest of the crater Lermontov (Robinson and Lucey, 1997).

Additional candidates for pyroclastic deposits on Mercury were revealed by images obtained by MESSENGER during the spacecraft's first flyby. Along the southern edge of the Caloris basin are a number of diffuse-edged deposits having a distinct reddish color with respect to the general Mercury continuum. Many of these deposits are associated with irregular depressions (Fig. 1) (Head et al., 2008; Murchie et al., 2008; Robinson et al., 2008; Head et al., 2009a-this issue).

The largest of these features interpreted as pyroclastic deposits, located just inside the southwestern rim of Caloris, is shown in Fig. 2. Fig. 2A and D were produced with the Integrated Software for Imaging Spectrometers (ISIS) software package developed by the United States Geological Survey (USGS) from images EN0108826812M and EN0108826877M, which were acquired by the Mercury Dual Imaging System (MDIS) narrow-angle camera (NAC) (Hawkins et al., 2007) and then calibrated and referenced to planetary coordinates. With ArcGIS, a geographic information system software package, the images were converted to sinusoidal projection with a central meridian centered on the candidate vent. The digital number (DN) values in Fig. 2A were given a color scale to produce Fig. 2D. In Fig. 2C, a color mosaic from the multispectral wide-angle camera (WAC) of MDIS was placed in the same projection and overlaid on the higher-resolution NAC images. Multispectral images in 11 filters collected by the WAC were calibrated to irradiance/solar flux (I/F) and photometrically adjusted to the standard bidirectional geometry of 30° solar incidence and 0° emission angle (Robinson et al., 2008; Blewett et al., 2009-this issue).

The feature (centered at 22°N, 146°E) consists of an approximately 20-km-long and 12-km-wide kidney-shaped depression surrounded by a bright, quasi-circular deposit of material having a diffuse boundary (Fig. 2A–D). Morphological evidence, especially the overall shading in the region around the kidney-shaped depression, suggests that the depression is at or near the summit of a subtle dome-like structure, which we interpret as a low shield volcano with a central vent that has given rise to a pyroclastic fall deposit having a higher albedo than the shield volcano and its surroundings (Fig. 2D, Head et al., 2008, 2009a-this issue). Directly to the southwest, and making up part of the general volcanic region described by Head et al. (2008), there is an adjoining smaller and more diffuse deposit, again interpreted to be pyroclastic, with similar color and high albedo, which may have been derived from one of the several vent-like depressions in the area (Fig. 2B). In addition to the irregular pits interpreted to be endogenic (Head et al., 2008), some crater-like rimless pits are seen, which is consistent with the style of impact craters emplaced into pyroclastic deposits on the Moon (Lucchitta and Schmitt, 1974).

The diffuse deposit is identified as pyroclastic on the basis of three lines of evidence. First, it has diffuse boundaries, similar to those seen at the outer margins of deposits on Io known from observations to be fall deposits (Strom et al., 1981). Second, the near-circularity of the deposit and the coincidence of its center of symmetry with the kidney-shaped depression are entirely consistent with the dispersal of ballistically transported pyroclasts from a vent within the depression. Finally, the anomalous color signature of the deposit in multispectral images (Head et al., 2008; Murchie et al., 2008; Robinson et al., 2008) suggests a coherent layer of material with physical or chemical properties differing from those of the pre-existing surface rocks in this region.

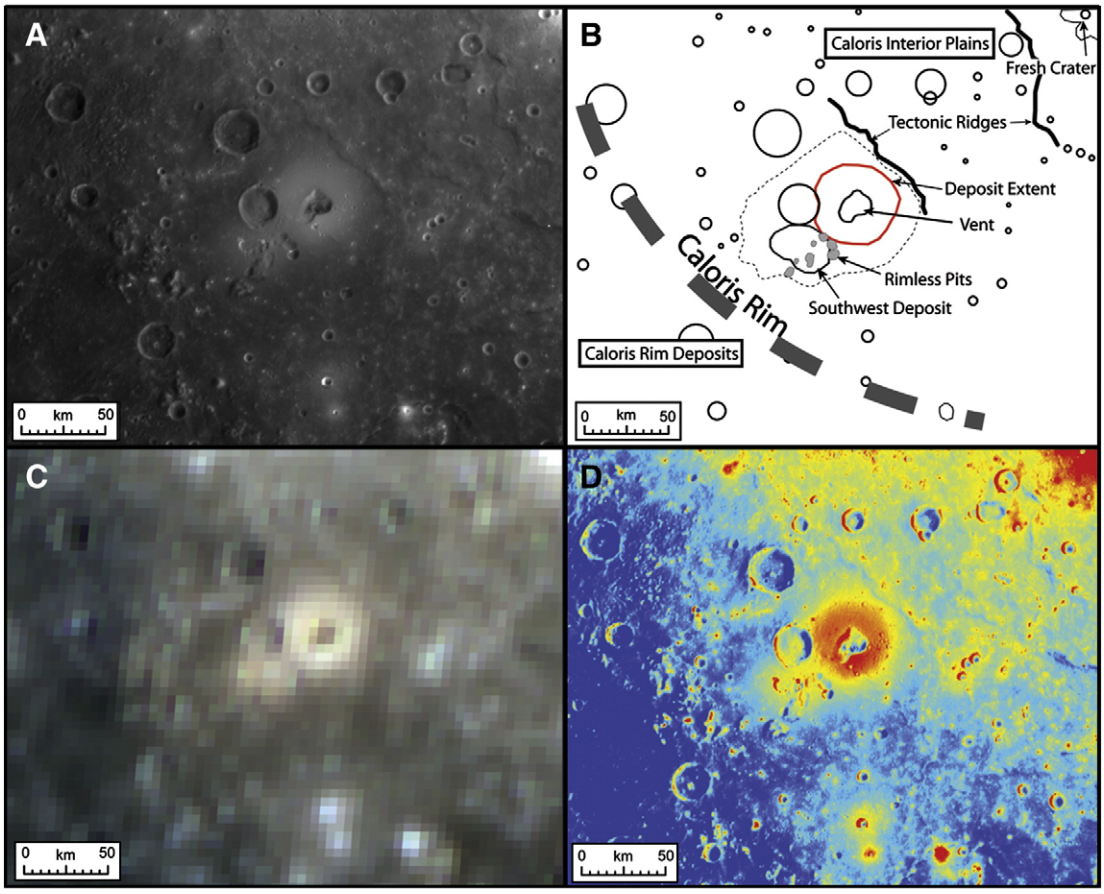

Fig. 2. (A) The feature in box A from Fig. 1 possesses a shield-like structure, central kidney-shaped depression, and surrounding bright deposit interpreted to be pyroclastic in origin (Head et al., 2008, 2009a-this issue). From MDIS NAC images EN0108826812M and EN0108826877M. (B) A sketch map showing the general geological units of the area. The red outline marks the approximate boundary of the main deposit, determined from color and albedo data, with an average radius of approximately 24 km. The smaller feature to the southwest appears to have similar color and morphological characteristics and is probably a pyroclastic deposit associated with one of the other irregular depressions. (C) A WAC RGB image (red = 480 nm, green = 750 nm, blue = 1000 nm) for the area. (D) Color-coded albedo map of the area, derived from the NAC image in (A). Albedo increases from blue (low values) to red (highest values). The albedo varies because of variations in composition, illumination due to topography, and viewing angle. The deposit is brighter on the southeastern side, as expected if the feature were slightly domical. See Head et al. (2008, 2009a-this issue) for additional discussion on the topography.

The main deposit, also identified as Red Spot 3 by Blewett et al. (2009-this issue), has a reflectance at 750 nm of 0.082. While all of the red spots have spectra with relatively consistent shape, this deposit has an albedo not only higher than the plains that surround it but also higher than the other red spots (Blewett et al., 2009-this issue). The albedo of this deposit nonetheless appears to fall within the general range for lunar pyroclastic deposits, as specified by Gaddis et al. (2003). Fig. 3 shows the spectrum of the candidate pyroclastic deposit compared with the spectra of several lunar pyroclastic deposits. The deposit is comparable in reflectance to the J. Herschel deposit and a deposit on the rim of Orientale (Head et al., 2002) and would appear dark compared with lunar highland soils (Pieters and Tompkins, 1999). However, like other spectra from Mercury, this spectrum lacks a downturn starting near 750 nm that represents the beginning of the 1000-nm ferrous iron band (Blewett et al., 2002; Warell and Blewett, 2004; Robinson et al., 2008; Blewett et al., 2009-this issue). The brightness and redness of the spectrum suggest that the opaque content is low compared with the average surface in the region of Mercury seen by MESSENGER. Fig. 4 shows the spectra of other nearby features on Mercury relative to the spectrum of the candidate deposit. The deposit is brighter than the circum-Caloris plains (which have low reflectance compared with the lunar highlands and maria) and the Caloris interior plains, (which have low reflectance compared with the lunar highlands and similar reflectance compared with the lunar maria). The southwestern deposit has spectral characteristics intermediate between those of the main deposit and those of the inner Caloris plains (Fig. 4). This would be expected if the southwestern deposit represented a thin pyroclastic layer emplaced on interior plains material. The spectrum of the pyroclastic deposit is red compared with that of immature crater material.

5. Vent eruption speed

From the radial extent of the pyroclastic deposits, we may estimate the eruption speed at the central vent. We chose the center of the kidney-shaped depression to be the location of the vent, and we mapped the perimeter of the hypothesized pyroclastic unit on the basis of its distinctive color (Fig. 2C) (Head et al., 2008; Murchie et al., 2008; Robinson et al., 2008). We excluded the smaller southwestern deposit identified in Head et al. (2008) from the analysis on the basis that it was not likely to be derived from the same source. We took 23 transects to determine an average radius of the deposit of 24 km, with a standard deviation of 2 km, in agreement with the radius of ~25 km originally given by Head et al. (2008). This radius represents the edge of the deposit and thus the greatest distance that a pyroclast would have to travel from the vent.

The maximum range of a pyroclast may then be used to estimate its eruption speed. On a planet with an atmosphere, the speed of erupting pyroclasts is greatly slowed by interaction between the volcanic gas and clasts and the molecules that compose the atmosphere.

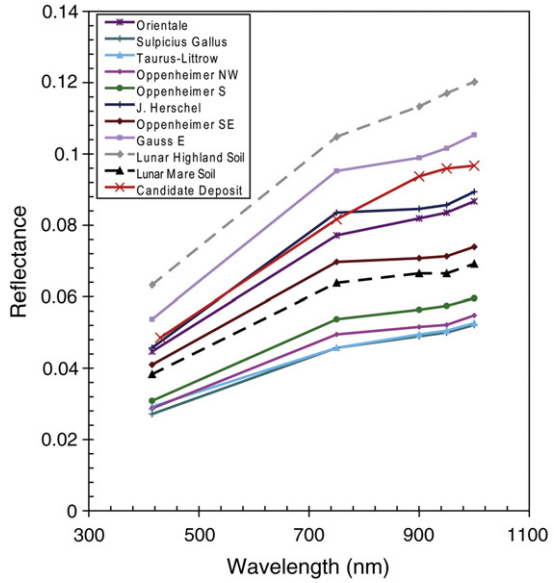

Fig. 3. The spectrum of the candidate pyroclastic deposit (red curve) taken from the multispectral WAC images compared with spectra of pyroclastic deposits on the Moon (from Gaddis et al., 2003) and soils from the lunar highlands and maria (near Tsiolkovsky crater) for reference (from Pieters and Tompkins, 1999). The spectrum of the candidate deposit represents an average of ~10 individually selected pixels taken from around the vent. All spectra were corrected for phase angle and calibrated to absolute reflectance. The Hillier et al. (1999) correction was applied to the Clementine spectra. Bands that were not shared between the two data sets were not included, except for the 415-nm band of Clementine and the 430-nm band of MESSENGER in order to illustrate the visible continuum. The spectrum of the candidate Mercury deposit is similar in absolute reflectance to those of some of the brighter lunar pyroclastic deposits, but it clearly differs in composition, specifically because of the absence of any resolvable mafic absorption near 1000 nm.

The drag imparted by the atmosphere dissipates the energy of the eruption and results in a lower, more collimated fire fountain. On a body with no atmosphere, such as Mercury or the Moon, clasts emerging from the vent interact only with the volcanic gas entraining

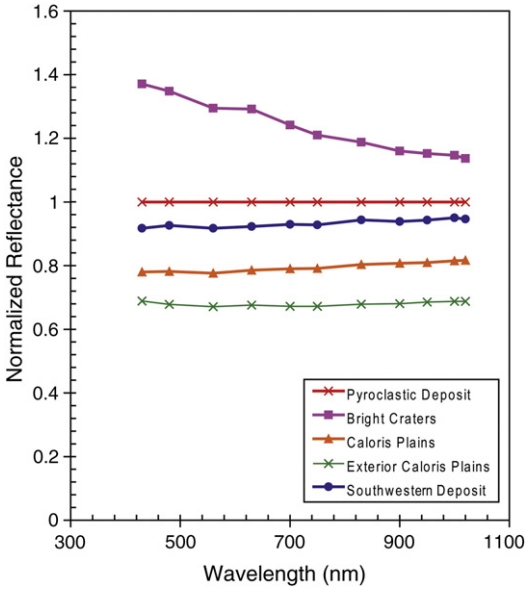

Fig. 4. Spectra taken from the features labeled in Fig. 2B and normalized to the spectrum of the candidate pyroclastic deposit to emphasize differences. The spectra represent averages of ~10 individually selected pixels on each surface type. The spectrum for the southwestern deposit appears to be a combination of that for the pyroclastic deposit and that for the Caloris interior plains unit, suggesting that the plains can be seen through the thin pyroclastic deposit.

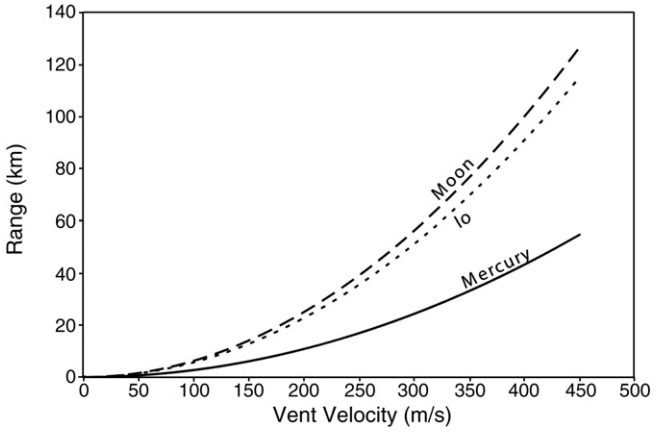

Fig. 5. A comparison of pyroclast range as a function of vent velocity for Mercury, Io, and the Moon showing how maximum range changes with acceleration due to gravity.

them (Wilson and Head, 1981). The volcanic gas quickly decompresses to the point where gas-particle interactions become negligible, leaving the pyroclasts to follow ballistic trajectories back to the surface (Head and Wilson, 1979; Wilson and Keil, 1997). In addition to the absence of drag from the atmosphere, explosive eruptions on bodies with very low atmospheric pressure should lead to more widespread pyroclast dispersal because of the acceleration of the gas as it expands from its initial pressure in the vent to the essentially zero external pressure.

Large pyroclasts may fall back around the mouth of the vent or back into the vent itself, but small pyroclasts (less than ~2 cm) will have terminal velocities in the upward-moving gas that are negligible compared with the gas velocity, meaning that the clasts have an ejection velocity effectively equal to the velocity of the gas (Wilson and Head, 1981; Wilson and Keil, 1997). The range of a pyroclast may be calculated from its ballistic trajectory:

$$X = \frac{v^2}{g}\sin 2\theta, \tag{1}$$

where X is the maximum horizontal distance travelled by the pyroclast, v is the velocity at the vent, g is the gravitational acceleration at the surface of the body (3.7 m/s^2 on Mercury), and θ is the angle of ejection of the pyroclasts from the vent, measured from the zenith. The maximum dispersal of pyroclasts would take place at an ejection angle of 45°. By Eq. (1), this condition and a range of $X = 24$ km gives a

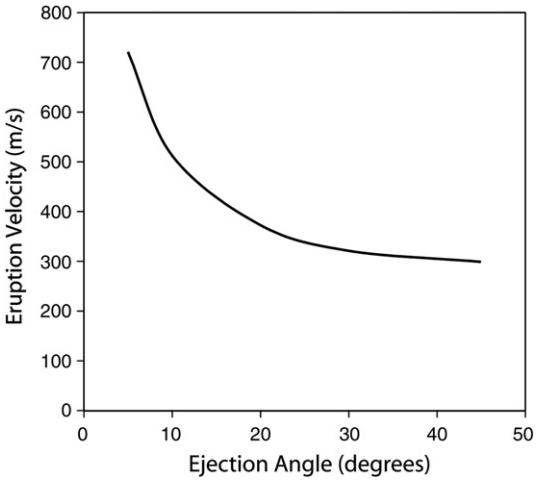

Fig. 6. The effect of the ejection angle on the pyroclast eruption velocity needed for pyroclasts to reach the edge of the observed deposit.

minimum vent velocity of ~300 m/s. The range is inversely proportional to the acceleration due to gravity, leading to different maximum dispersals on different airless bodies (Fig. 5). In reality, the eruption angle of the clasts will generally be less than the optimum 45° because the vent would not necessarily have the appropriate shape to enable pressure-balanced flow, and the flow would thus become choked (Wilson and Head, 2001). A smaller or larger angle would require a greater eruption velocity in order for the clasts to reach the edge of the deposit (Fig. 6). Over time, the erosional force of the volcanic jet coupled with coarse clast deposition around the vent may modify the volcanic opening until it reaches the ideal geometry (Wilson and Keil, 1997).

6. Thermal state of the fire fountain

As clasts are expelled into space, they lose heat to their surroundings depending on the optical density of the particles (and thus the level to which they are exposed to the surrounding environment, in this case a cold vacuum) (Wilson and Head, 2001). If they are shielded by other pyroclasts (i.e., the fire fountain has a high optical density), they will remain hotter longer, which could allow time for crystals to form (Wilson and Head, 2001). To quantify this effect, Wilson and Keil (1997) derived a relation for the distance, Λ, into the pyroclastic droplet cloud that ensures almost complete obscuration from the outside (for a circular vent):

$$\Lambda = \frac{\left(\pi\phi v^3\right)(1 - \cos\theta)X}{3GVg}, \quad (2)$$

where ϕ is the diameter of the pyroclasts, G is a parameter describing the droplet size distribution (how large the largest clasts are with respect to the mean), and V is the volume flux of magma being erupted from the vent. All else being equal, Mercury will have fire fountains with a higher optical density than those on Io or the Moon because of its higher gravitational acceleration. This means that the pyroclasts will be more sheltered from the vacuum and will remain warm for a longer period of time before their deposition on the surface. Additionally, the flight times of pyroclasts on the Moon and Io will be longer because of the lower gravity, and thus more of the exposed pyroclasts will fall to the surface cold.

These thermal differences may cause differences in morphology or albedo, as a warm layer of pyroclasts from the inner parts of the fountain could weld, coalesce, or flow after emplacement (Head and Wilson, 1989). The greater shielding of the pyroclasts on Mercury would allow beads to cool more slowly, allowing more crystallization to take place rather than immediate quenching as glasses. As mentioned above, higher-albedo orange spheres on the Moon were found to be quenched glasses, while lower-albedo black beads represent their partially crystallized equivalents (Heiken et al., 1974). However, if ejected magma droplets on Mercury were low in opaque minerals, it is possible that the crystallized beads would not be dark like those observed on the Moon. If the pyroclastic material is low in titanium, the volcanic glasses could have a higher albedo similar to that of the Apollo 15 green glasses (Bell et al., 1976; Lucey et al., 1998).

7. Comparisons with lunar pyroclastic deposits and inferred magma volatile contents

With an average radius of ~24 km, the candidate pyroclastic deposit on Mercury is larger than 80% of documented pyroclastic deposits on the Moon (Gaddis et al., 2003). Scaled to reflect the Moon's lower gravity, the deposit resulting from pyroclasts ejected at this speed would be the third largest pyroclastic deposit on the Moon, with an area of approximately 9800 km^2 (Gaddis et al., 2003). The other anomalous features around the Caloris rim with similar properties in the principal component image (Fig. 1, orange areas) are either comparable in size (but more diffuse) or smaller than the vent analyzed here (Murchie et al., 2008; Head et al., 2008, 2009a-this issue). Like many lunar pyroclastic deposits, these features appear to be concentrated around the rim of a large impact basin, suggesting a possible structural control on their emplacement. However, infilling of the Caloris interior by lava flows (smooth plains volcanism) could have preferentially obscured other, more centrally located pyroclastic deposits.

Any explosively erupting magma on Mercury would require a higher mass fraction of volatiles than on the Moon in order to emplace pyroclasts to a given distance. To quantify this effect, we note that the range is proportional to v^2/g (Eq. (1)) and hence directly proportional to the kinetic energy. However, to a very close approximation the kinetic energy of the eruption products is itself directly proportional to the released magma gas mass fraction, f (Wilson, 1980), and so range is directly proportional to f/g. Wilson and Head (1981) determined that ~500 ppm of CO (a vent speed of 90 m/s) would be needed to eject pyroclasts to a range of 5 km on the Moon. The f/g scaling then implies that emplacing clasts to 24 km from a vent on Mercury would require ~5500 ppm of CO. To emplace clasts to the same 24 km range on the Moon, only 2400 ppm would be required, less than half that required for Mercury. Table 1 shows the magmatic abundances of candidate volatiles needed to emplace clasts to a distance of 24 km on the Moon and Mercury (both for a 45° ejection angle). The volatile fraction depends on the volatile assumed, because the energy available from gas expansion is inversely proportional to the molecular mass of the volatile.

Uncertainties in these calculations include the ejection angle of the particles and the possibility that the central vent is composed of several overlapping vents, which could decrease the range. While an ejection angle of 45° is assumed to calculate the minimum required exit velocity and volatile content, the ejection angle is uncertain both for the deposit on Mercury and for those on the Moon. For example, if the pyroclasts on the Moon were ejected at a 45° angle, but the pyroclasts on Mercury were ejected at a 30° or 60° angle, the required magmatic volatile content for the eruption on Mercury would increase by about 13%. In the case of range uncertainty because of several overlapping vents or other factors, a 5 km reduction in range would correspond to a reduction of about 16% in the required volatile content.

In order to determine which of these volatiles is most likely to have driven pyroclastic eruptions on Mercury, several lines of argument may be taken into consideration. First, common magma volatiles on other planetary bodies from which samples are available (namely, the Earth, the Moon, and meteorite parent bodies) may be considered. Pyroclastic eruptions on the Earth are mainly propelled by H_2O, CO_2, and SO_2. On the Moon CO_2 and SO_2 are less common because of the reducing state of the lunar interior, and H_2O is highly depleted, though it is present in small amounts (Saal et al., 2008). Lunar pyroclastic eruptions have been shown to be driven mainly by CO created during ascent by means of reactions between graphite and FeO to produce metallic iron and $CO + CO_2$ gas (Sato, 1976; Fogel and Rutherford, 1995; Rutherford and Papale, 2009). In the absence of FeO, elemental carbon may also reduce other oxide components of the silicate melt (Ni, Co, and even Si) to form CO and CO_2 as the magma ascends. Enstatite chondrites, which are thought to have similar composition to

Table 1
Magmatic abundances of various types of volatiles required to emplace pyroclasts to an equivalent range (24 km) on Mercury and the Moon.

	Mercury	Moon
CO	5500 ppm	2400 ppm
CO_2	8700 ppm	3800 ppm
H_2O	3600 ppm	1600 ppm
SO_2	13000 ppm	5600 ppm

the parent body of the low-Fe aubrites (igneous enstatite chondrites formed under highly reducing conditions), have been suggested to contain CO in tiny cracks and microvesicles in lieu of complete dissolution in the silicate matrix (Muenow et al., 1992). The amount of CO that was found (1580–2830 ppm) could be sufficient to drive a small pyroclastic eruption (Muenow et al., 1992), but it is unclear whether this process would apply on Mercury.

On the basis of redox state alone, we would expect oxidized gases such as CO_2 and SO_2 to dominate for a more oxidized interior, and reduced gases such as CO and H_2S for a more reduced interior. H_2O may be present in either case. The solubility of sulfur and its speciation into sulfide or oxide are complex functions of oxygen fugacity, pressure, temperature, magmatic water, and other constituents. Gerlach (1986) asserted that the overall solubility of sulfur as a function of pressure is similar to that of H_2O, and Haughton et al. (1974) measured solubilities at one atmosphere that varied from 0.05 to 0.2 wt.% as the Fe content of a mafic magma increased from 5% to 20%. Thus if low-Fe melts are predominant on Mercury, we can reasonably assume that at least ~0.05%, i.e., 500 ppm, S is released by the time the magma expands to vacuum. If this S were released as H_2S, then because the molecular weights of H_2S and S are similar the weight fraction of H_2S will also be close to 500 ppm.

However, whether the interior of Mercury is oxidizing or reducing, the exsolution of volatiles such as S requires that the initial gas phase be generated in the ascending magma as either H_2O or CO_2 (and CO); S species would then partition into the C–O–H gas (Sato, 1976; Nicholis and Rutherford, 2005). Thus the presence of pyroclastic volcanism on Mercury requires either H_2O or CO to be available, although CO can be created by oxidation during the ascent and does not need to be originally dissolved in the melt (Sato, 1976; Fogel and Rutherford, 1995; Rutherford and Papale, 2009). The presence of any significant amount of water in the melt would be a somewhat unexpected result for reasons discussed below. The actual gas driving the pyroclastic eruptions on Mercury will most likely be a combination of several volatiles, including S.

For Earth, the Moon, and meteorite parent bodies, the concentration of common magmatic volatiles found in basalt samples is somewhat less than the values calculated in Table 1 (except in the case of H_2O on Earth, which can be up to several wt. %). However, relatively insoluble CO and CO_2 partition into the vapor phase even at fairly high pressures (Wallace and Anderson, 2000). Much of this gas would escape upon eruption or degassing and would not be preserved in the solidified magma. In some cases, magma residing for extended periods of time in a shallow reservoir can exsolve volatiles and build up a foam, the collapse of which leads to an eruption that is artificially gas-rich. An extreme case of this can occur in the high-pressure environment of Earth's seafloor (Head and Wilson, 2003). For a submarine pyroclastic eruption taking place at 500 m depth, ~8000 ppm H_2O or ~19,000 ppm CO_2 would be needed to emplace pyroclasts to the distances that they have been observed on the seafloor, much of this probably provided by the concentration of gases over time in the reservoir (Head and Wilson, 2003). The Mercury environment lies at the low-pressure end of the range of possibilities, where this process will produce lower gas concentrations. However, the fact that some volatile concentration is possible leads us to consider the volatile contents derived here to be upper limits on abundances in the primary magma.

8. Discussion

The deposit studied here, if correctly interpreted as pyroclastic in origin, represents a large eruption requiring a substantial magmatic volatile content, in the range 3600–13,000 ppm for a variety of candidate volatiles (Table 1). These values are comparable to or larger than the volatile contents of terrestrial oceanic basalts. The best estimates of mantle volatile content on Earth come from basalts erupted at mid-ocean ridges and oceanic hotspots. The absolute water contents of mid-ocean ridge basalt (MORB) glasses and their melt inclusions are 400–1600 ppm, while the upper mantle water content is estimated at ~150 ppm and that for the bulk Earth at ~350 ppm (Sobolev and Chaussidon, 1996; Saal et al., 2002; Marty and Yokochi, 2006). Measurements of the exsolution of volatiles from basaltic eruptive episodes at Kilauea volcano, Hawaii, indicate values of ~3000 ppm H_2O, ~6500 ppm CO_2, and ~1300 ppm S (Gerlach, 1986) for the hotspot mantle source.

Such high volatile contents in the interior of Mercury, even locally, are at variance with most theories for the planet's formation. Several hypotheses have been advanced to account for Mercury's high bulk density and current solar distance, including fractionation of silicates from metal by aerodynamic drag in the early, hot, inner solar nebula (Weidenschilling, 1978) and removal of a large fraction of the planet's silicate shell after global differentiation, either by vaporization in the hot nebula (Cameron, 1985; Fegley and Cameron, 1987) or by disruption during a giant impact (Wetherill, 1988; Benz et al., 1988, 2007). All such models involve one or more sustained episodes of high temperatures that would leave Mercury extremely depleted in volatile materials relative to cosmic abundances and even to the other inner planets (Boynton et al., 2007).

There are several possible variants of formation theories that might permit a larger inventory of volatiles in Mercury's interior. It is possible, although unlikely, that Mercury largely accreted at a greater solar distance than it currently occupies, on the grounds that objects of Mercury's mass (5% of Earth's mass) can experience major excursions in their semi-major axis during the gravitational interactions among planetesimals and planetary embryos prior to the final assembly of the inner planets (Wetherill, 1988). Moreover, meteorite chemical arguments suggest that temperatures in the solar nebula throughout the distance range of the terrestrial planets were too hot for hydration of planetesimals and that the inventory of water on the Earth and other terrestrial planets came primarily from water-rich embryos that formed farther from the Sun and were scattered inward by interactions with the gas-giant planets (Morbidelli et al., 2000). Simulations of water accretion by this process permit the incorporation of some water, and presumably other volatiles, even for the innermost planet (e.g., Raymond et al., 2004), although a strong sensitivity to the formation times and early positions of the gas-giant planets and the generally stochastic character of the required gravitational interactions render impossible the prediction of volatile inventories for specific bodies. A giant impact onto Mercury would have resulted in widespread loss of volatiles from the planet's silicate shell, but the partial re-accretion of material ejected into solar orbit (Benz et al., 2007) could have returned a small fraction of the lost volatiles. Moreover, the recent discovery of water in pyroclastic glass samples from the Moon (Saal et al., 2008), a body thought to have formed at high temperatures following a giant impact (Canup, 2006), suggests that the relation between formation process and interior volatile budget may be more complex for both Mercury and the Moon than previously appreciated.

There is growing evidence that at least the surface of Mercury is not volatile-depleted. The exosphere includes the moderately volatile alkali metals sodium (Potter and Morgan, 1985) and potassium (Potter and Morgan, 1986); the polar deposits in the floors of permanently shadowed near-polar craters are thought to consist of water ice (Harmon and Slade, 1992; Slade et al., 1992) or perhaps elemental sulfur (Sprague et al., 1995), and the Fast Imaging Plasma Spectrometer (FIPS) on MESSENGER detected water-group and sulfur-group ions during the spacecraft's first Mercury flyby (Zurbuchen et al., 2008). The fraction of Mercury's exospheric sodium and potassium derived from material indigenous to Mercury's crust is not well known, however. Models of the sodium exosphere, for instance, indicate that the influx of micrometeoroids may be sufficient to balance sodium loss (Leblanc and Johnson, 2003). Suggestions that particular features on Mercury's surface may be sources for enhanced release of potassium (Sprague et al., 1990) or sodium (Sprague and Massey, 2007) would, if

verified, considerably strengthen the case for alkali metals in crustal material. The polar deposits, too, need not necessarily provide information on interior volatiles. Their distribution can be accommodated by the influx of micrometeoroids or the impact of comparatively recent comets or volatile-rich asteroids, with subsequent migration of volatiles to polar cold traps (Moses et al., 1999). The enhanced radar backscatter of the deposits is best matched by a regolith-covered layer of clean ice having characteristics consistent with emplacement within the last several tens of millions of years (Crider and Killen, 2005). The water and sulfur group ions detected in Mercury's ionized exopshere by FIPS may be derived from like neutral species at Mercury's surface, but they may alternatively be supplied by micrometeoroid impact or chemical sputtering (Zurbuchen et al., 2008). The inference from imaged volcanic features that Mercury experienced pyroclastic eruptions and therefore contains substantial interior volatiles at least on the scale of selected magma source regions provides new information with which to interpret the evidence for volatiles at Mercury's surface.

9. Conclusions

We have presented evidence for the presence of significant amounts of volatiles in partial melts derived from the interior of Mercury at one volcanic site at the margin of the Caloris basin and, by extrapolation, at other sites that display comparable morphological and spectral characteristics (Murchie et al., 2008; Head et al., 2009a-this issue). Such a result favors a formation history that allows for the accretion of volatile-rich planetesimals, e.g., from the outer solar system, and the retention of at least some of those volatiles through planetary growth and the creation of Mercury's anomalously high ratio of metal to silicate. This finding also provides a fresh constraint on sources of volatile species in Mercury's polar deposits and in the planet's neutral and ionized exosphere.

There is growing evidence that volcanism was an important process in Mercury's geological evolution, at least early in the planet's history (Head et al., 2008, 2009a-this issue, 2009b-this issue; Gillis-Davis et al., 2009-this issue). That some volcanic eruptions on Mercury were explosive is an important aspect of that history, but at this point the geographic distribution of pyroclastic deposits is not fully known, and the relative importance of explosive and effusive eruptions in Mercury's volcanic history is poorly constrained. Better documentation of the distribution and volumes of volcanic materials from both types of eruptions will provide insight into the questions of whether magmatic volatile contents similar to those inferred in this paper were common or rare and therefore the degree of heterogeneity of volatile abundances in Mercury's magma source regions as functions of position and time. The answers to these questions will inform a broad sweep of topics ranging from the degree of mixing within Mercury's interior following planet formation to the history of outgassing from the planet's interior.

Pyroclastic deposits on Mercury provide a new and important source of information on the general topic of explosive eruptions on airless bodies. By comparison with pyroclastic deposits on the Moon and Io, the influence of such factors such as magmatic composition, the abundance of darkening agents such as Fe and Ti, grain size, and emplacement history on the final spectral character of pyroclastic deposits on solid solar system objects can be better understood.

Acknowledgements

The MESSENGER project is supported by the NASA Discovery Program under contracts NASW-00002 to the Carnegie Institution of Washington and NAS5-97271 to the Johns Hopkins University Applied Physics Laboratory. We thank Brett Denevi for providing calibrated WAC image products. This paper benefited from fruitful discussions with Peter Isaacson, Carle Pieters, and Malcolm Rutherford.

References

Bell, P.M., Mao, H.K., Weeks, R.A., 1976. Optical spectra and electron paramagnetic resonance of lunar and synthetic glasses: a study of the effects of controlled atmosphere, composition, and temperature. Proc. Lunar Planet. Sci. Conf. 7, 2543–2559.
Benz, W., Slattery, W.L., Cameron, A.G.W., 1988. Collisional stripping of Mercury's mantle. Icarus 74, 516–528.
Benz, W., Anic, A., Horner, J., Whitby, J.A., 2007. The origin of Mercury. Space Sci. Rev. 132, 189–202.
Blewett, D.T., Hawke, B.R., Lucey, P.G., 2002. Lunar pure anorthosite as a spectral analog for Mercury. Meteorit. Planet. Sci. 37, 1245–1254.
Blewett, D.T., Hawke, B.R., Lucey, P.G., Robinson, M.S., 2007. A Mariner 10 color study of Mercurian craters. J. Geophys. Res. 112, E02005. doi:10.1029/2006JE002713.
Blewett, D.T., Robinson, M.S., Denevi, B.W., Gillis-Davis, J.J., Head, J.W., Solomon, S.C., Holsclaw, G.M., McClintock, W.E., 2009. Multispectral images of Mercury from the first MESSENGER flyby: analysis of global and regional color trends. Earth Planet. Sci. Lett., this issue.
Boss, A.P., 1998. Temperatures in protoplanetary disks. Annu. Rev. Earth Planet. Sci. 26, 53–80.
Boynton, W.V., Sprague, A.L., Solomon, S.C., Starr, R.D., Evans, L.G., Feldman, W.C., Trombka, J.I., Rhodes, E.A., 2007. MESSENGER and the chemistry of Mercury's surface. Space Sci. Rev. 131, 85–104.
Burns, R.G., 1993. Origin of electronic spectra of minerals in the visible to near-infrared region. In: Pieters, C.M., Englert, P. (Eds.), Remote Geochemical Analysis: Elemental and Mineralogical Composition. Cambridge Univ. Press, Cambridge, UK, pp. 3–27.
Cameron, A.G.W., 1985. The partial volatilization of Mercury. Icarus 64, 285–294.
Canup, R.M., 2006. Simulations of a late lunar-forming impact. Icarus 168, 433–456.
Chambers, J.E., 2005. Planet formation. In: Davis, A.M. (Ed.), Meteorites, Comets and Planets, Treatise on Geochemistry, vol. 1. Elsevier, New York, pp. 461–475.
Coombs, C.R., Hawke, B.R., Lucey, P.G., Owensby, P.D., Zisk, S.H., 1990. The Alphonsus region: a geologic and remote sensing perspective. Proc. Lunar Planet. Sci. Conf. 20, 161–174.
Crider, D., Killen, R.M., 2005. Burial rate of Mercury's polar volatile deposits. Geophys. Res. Lett. 32, L12201. doi:10.1029/2005GL022689.
Delano, J.W., 1986. Pristine lunar glasses: criteria, data, and implications. Proc. Lunar Sci. Conf. 16, D201–213.
Fegley, B., Cameron, A.G.W., 1987. A vaporization model for Fe/Si fractionation in the Mercury protoplanet. Earth Planet. Sci. Lett. 82, 207–222.
Fogel, R.A., Rutherford, M.J., 1995. Magmatic volatiles in primitive lunar glasses: I. FTIR and EPMA analyses of Apollo 15 green and yellow glasses and revision of the volatile-assisted fire-fountain theory. Geochim. Cosmochim. Acta 59, 201–215.
Gaddis, L.R., Pieters, C.M., Hawke, B.R., 1985. Remote sensing of lunar pyroclastic mantling deposits. Icarus 61, 461–489.
Gaddis, L.R., Staid, M.I., Tyburczy, J.A., Hawke, B.R., Petro, N.E., 2003. Compositional analyses of lunar pyroclastic deposits. Icarus 161, 262–280.
Gerlach, T.M., 1986. Exsolution of H_2O, CO_2, and S during eruptive episodes at Kilauea Volcano, Hawaii. J. Geophys. Res. 91, 12177–12185.
Gillis-Davis, J.J., Blewett, D.T., Gaskell, R.W., Denevi, B.W., Robinson, M.S., Strom, R.G., Solomon, S.C., Sprague, A.L., 2009-this issue. Pit-floor craters on Mercury: evidence of near-surface igneous activity. Earth Planet. Sci. Lett. doi:10.1016/j.epsl.2009.05.023.
Hapke, B., 2001. Space weathering from Mercury to the asteroid belt. J. Geophys. Res. 106, 10039–10073.
Harmon, J.K., Slade, M.A., 1992. Radar mapping of Mercury: full-disk images and polar anomalies. Science 258, 640–643.
Haughton, D.R., Roeder, P.L., Skinner, B.J., 1974. Solubility of sulfur in mafic magmas. Econ. Geol. 69, 451–467.
Hawke, B.R., Coombs, C.R., Gaddis, L.R., Lucey, P.G., Owensby, P.D., 1989. Remote sensing and geologic studies of localized dark mantle deposits on the Moon. Proc. Lunar Planet. Sci. Conf. 19, 255–268.
Hawkins III, S.E., Boldt, J.D., Darlington, E.H., Espiritu, R., Gold, R.E., Gotwols, B., Grey, M.P., Hash, C.D., Hayes, J.R., Jaskulek, S.E., Kardian Jr., C.J., Keller, M.R., Malaret, E.R., Murchie, S.L., Murphy, P.K., Peacock, K., Prockter, L.M., Reiter, R.A., Robinson, M.S., Schaefer, E.D., Shelton, R.G., Sterner II, R.E., Taylor, H.W., Watters, T.R., Williams, B.D., 2007. The Mercury Dual Imaging System on the MESSENGER spacecraft. Space Sci. Rev. 131, 247–338.
Head, J.W., 1974. Lunar dark-mantle deposits: possible clues to the distribution of early mare deposits. Proc. Lunar Sci. Conf. 5, 207–222.
Head, J.W., 1976. Lunar volcanism in space and time. Rev. Geophys. Space Phys. 14, 265–300.
Head, J.W., Wilson, L., 1979. Alphonsus-type dark-halo craters: morphology, morphometry and eruption conditions. Proc. Lunar Planet. Sci. Conf. 10, 2861–2897.
Head, J.W., Wilson, L., 1989. Basaltic pyroclastic eruptions: influence of gas-release patterns and volume fluxes on fountain structure, and the formation of cinder cones, spatter cones, rootless flows, lava ponds and lava flows. J. Volcanol. Geotherm. Res. 37, 261–271.
Head, J.W., Wilson, L., 2003. Deep submarine pyroclastic eruptions: theory and predicted landforms and deposits. J. Volcanol. Geotherm. Res. 121, 155–193.
Head, J.W., Wilson, L., Weitz, C.M., 2002. Dark ring in southwestern Orientale basin: origin as a single pyroclastic eruption. J. Geophys. Res. 107, 5001. doi:10.1029/2000JE1438.
Head, J.W., Murchie, S.L., Prockter, L.M., Robinson, M.S., Solomon, S.C., Strom, R.G., Chapman, C.R., Watters, T.R., McClintock, W.E., Blewett, D.T., Gillis-Davis, J.J., 2008. Volcanism on Mercury: evidence from the first MESSENGER flyby. Science 321, 69–72.
Head, J.W., Murchie, S.L., Prockter, L.M., Solomon, S.C., Chapman, C.R., Strom, R.G., Watters, T.R., Blewett, D.T., Gillis-Davis, J.J., Fassett, C.I., Dickson, J.L., Morgan, G.A., Kerber, L., 2009a-this issue. Volcanism on Mercury: evidence from the first

MESSENGER flyby for extrusive and explosive activity and the volcanic origin of plains. Earth Planet. Sci. Lett. doi:10.1016/j.epsl.2009.03.007.
Head, J.W., Murchie, S.L., Prockter, L.M., Solomon, S.C., Strom, R.G., Chapman, C.R., Watters, T.R., Blewett, D.T., Gillis-Davis, J.J., Fassett, C.I., Dickson, J.L., Hurwitz, D.M., Ostrach, L.R., 2009b-this issue. Evidence for intrusive activity on Mercury from the first MESSENGER flyby. Earth Planet. Sci. Lett. doi:10.1016/j.epsl.2009.03.008.
Heiken, G.H., McKay, D.S., Brown, R.W., 1974. Lunar deposits of possible pyroclastic origin. Geochim. Cosmochim. Acta 38, 1703–1718.
Hillier, J.K., Buratti, B.J., Hill, K., 1999. Multispectral photometry of the Moon and absolute calibration of the Clementine UV/Vis camera. Icarus 141, 205–225.
Leblanc, F., Johnson, R.E., 2003. Mercury's sodium exosphere. Icarus 164, 261–281.
Lucchitta, B.K., Schmitt, H.H., 1974. Orange material in the Sulpicius Gallus Formation at the southwestern edge of Mare Serenitatis. Proc. Lunar Sci. Conf. 5, 223–234.
Lucey, P.G., Hawke, B.R., Pieters, C.M., Head, J.W., McCord, T.B., 1986. A compositional study of the Aristarchus region of the Moon using near-infrared reflectance spectroscopy, J. Geophys. Res. 91, D344–D354.
Lucey, P.G., Taylor, G.J., Malaret, E., 1995. Abundance and distribution of iron on the Moon. Science 268, 1150–1153.
Lucey, P.G., Blewett, D.T., Hawke, B.R., 1998. Mapping the FeO and TiO_2 content of the lunar surface with multispectral imagery. J. Geophys. Res. 103, 3679–3699.
Marty, B., Yokochi, R., 2006. Water in the early Earth. Rev. Mineral. Geochem. 62, 421–450.
McClintock, W.E., Izenberg, N.R., Holsclaw, G.M., Blewett, D.T., Domingue, D.L., Head, J.W., Helbert, J., McCoy, T.J., Murchie, S.L., Robinson, M.S., Solomon, S.C., Sprague, A.L., Vilas, F., 2008. Spectroscopic observations of Mercury's surface reflectance during MESSENGER's first Mercury flyby. Science 321, 62–65.
Morbidelli, A., Chambers, J., Lunine, J.I., Petit, J.M., Robert, F., Valsecchi, G.B., Cyr, K.E., 2000. Source regions and timescales for the delivery of water to the Earth. Meteorit. Planet. Sci. 35, 1309–1320.
Moses, J.I., Rawlins, K., Zahnle, K., Dones, L., 1999. External sources of water for Mercury's putative ice deposits. Icarus 137, 197–221.
Muenow, D.W., Keil, K., Wilson, L., 1992. High-temperature mass spectrometric degassing of enstatite chondrites: implications for pyroclastic volcanism on the aubrite parent body. Geochim. Cosmochim. Acta 56, 4267–4280.
Murchie, S.L., Watters, T.R., Robinson, M.S., Head, J.W., Strom, R.G., Chapman, C.R., Solomon, S.C., McClintock, W.E., Prockter, L.M., Domingue, D.L., Blewett, D.T., 2008. Geology of the Caloris basin, Mercury: a view from MESSENGER. Science 321, 73–76.
Nicholis, M.G., Rutherford, M.J., 2005. Pressure dependence of graphite–C–O phase equilibria and its role in lunar volcanism. Lunar Planet. Sci. 36, abstract 1726.
Noble, S.K., Pieters, C.M., 2003. Space weathering on Mercury: implications for remote sensing. Solar Syst. Res. 37, 31–35.
Pieters, C.M., Tompkins, S., 1999. Tsiolkovsky crater: a window into crustal processes on the lunar farside. J. Geophys. Res. 104, 21935–21949.
Pieters, C.M., McCord, T.B., Charette, M.P., Adams, J.B., 1974. Lunar surface: identification of the dark mantling material in the Apollo 17 soil samples. Science 183, 1191–1194.
Pieters, C.M., Taylor, L.A., Noble, S.K., Keller, L.P., Hapke, B., Morris, R.V., Allen, C.C., McKay, D.S., Wentworth, S., 2000. Space weathering on airless bodies: resolving a mystery with lunar samples. Meteorit. Planet. Sci. 35, 1101–1107.
Potter, A.E., Morgan, T.H., 1985. Discovery of sodium in the atmosphere of Mercury. Science 229, 651–653.
Potter, A.E., Morgan, T.H., 1986. Potassium in the atmosphere of Mercury. Icarus 67, 336–340.
Rava, B., Hapke, B., 1987. An analysis of the Mariner 10 color ratio map of Mercury. Icarus 71, 397–429.
Raymond, S.N., Quinn, T., Lunine, J.I., 2004. Making other earths: dynamical simulations of terrestrial planet formation and water delivery. Icarus, 168, 1–17.
Robinson, M.S., Lucey, P.G., 1997. Recalibrated Mariner 10 color mosaics: implications for Mercurian volcanism. Science 275, 197–200.
Robinson, M.S., Murchie, S.L., Blewett, D.T., Domingue, D.L., Hawkins III, S.E., Head, J.W., Holsclaw, G.M., McClintock, W.E., McCoy, T.J., McNutt Jr., R.L., Prockter, L.M., Solomon, S.C., Watters, T.R., 2008. Reflectance and color variations on Mercury: regolith processes and compositional heterogeneity. Science 321, 66–69.
Rutherford, M.J., Papale, P., 2009. Origin of basalt fire-fountain eruptions on Earth versus the Moon. Geology 37, 219–222.
Saal, A.E., Hauri, E.H., Langmuir, C.H., Perfit, M.R., 2002. Vapor undersaturation in primitive mid-ocean ridge basalt and the volatile content of Earth's upper mantle. Nature 419, 451–455.
Saal, A.E., Hauri, E.H., Cascio, M.L., Van Orman, J., Rutherford, M.C., Cooper, R.F., 2008. The volatile content of the lunar volcanic glasses: evidence for the presence of water in the Moon's interior. Nature 454, 192–195.
Sato, M., 1976. Oxygen fugacity and other thermochemical parameters of Apollo 17 high-Ti basalts and their implications on the reduction mechanism. Proc. Lunar Planet. Sci. Conf. 7, 1323–1344.
Scott, D.H., McCauley, J.F., West, M.N., 1977. Geologic map of the west side of the Moon. Map I-1034, Misc. Investigations Ser. U.S. Geological Society, Denver, Colo.
Slade, M.A., Butler, B.J., Muhleman, D.O., 1992. Mercury radar imaging: evidence for polar ice. Science 258, 635–640.
Sobolev, A.V., Chaussidon, M., 1996. H_2O concentration in primary melts from supra-subduction zones and mid-ocean ridges: implications for H_2O storage and recycling in the mantle. Earth Planet. Sci. Lett. 137, 45–55.
Solomon, S.C., McNutt Jr., R.L., Watters, T.R., Lawrence, D.J., Feldman, W.C., Head, J.W., Krimigis, S.M., Murchie, S.L., Phillips, R.J., Slavin, J.A., Zuber, M.T., 2008. Return to Mercury: a global perspective on MESSENGER's first Mercury flyby. Science 321, 59–62.
Sprague, A.L., Massey, S.S., 2007. Mercury's exosphere: a possible source for Na. Planet. Space Sci. 55, 1614–1621.
Sprague, A.L., Kozlowski, R.W.H., Hunten, D.M., 1990. Caloris basin: an enhanced source for potassium in Mercury's atmosphere. Science 249, 1140–1143.
Sprague, A.L., Hunten, D.M., Lodders, K., 1995. Sulfur at Mercury, elemental at the poles and sulfides in the regolith. Icarus 118, 211–215.
Strom, R.G., Schneider, N.M., Terrile, R.J., Cook, A.F., Hansen, C., 1981. Volcanic eruptions on Io. J. Geophys. Res. 86, 8593–8620.
Vilas, F., 1988. Surface composition of Mercury from reflectance spectrophotometry. In: Vilas, F., Chapman, C.R., Matthews, M.S. (Eds.), Mercury. University of Arizona Press, Tuscon, Ariz., pp. 59–76.
Wallace, P.J., Anderson, A.T., 2000. Volatiles in magmas. In: Sigurdsson, H., Houghton, B., McNutt, S.R., Rymer, H., Stix, J. (Eds.), Encyclopedia of Volcanoes. Academic Press, San Diego, Calif., pp. 149–170.
Warell, J., 2003. Properties of the Hermean regolith: III. Disk-resolved vis-NIR reflectance spectra and implications for the abundance of iron. Icarus 161, 199–222.
Warell, J., Blewett, D.T., 2004. Properties of the Hermean regolith: V. New optical reflectance spectra, comparison with lunar anorthosites, and mineralogical modeling. Icarus 168, 257–276.
Warell, J., Sprague, J.P., Kozlowski, R.W.H., Long, A., 2006. The 0.7–5.3 μm IR spectra of Mercury and the Moon: evidence for high-Ca clinopyroxene on Mercury. Icarus 180, 281–291.
Weidenschilling, S.J., 1978. Iron/silicate fractionation and the origin of Mercury. Icarus 35, 99–111.
Weitz, C.M., Head, J.W., 1999. Spectral properties of the Marius Hills volcanic complex and implications for the formation of lunar domes and cones. J. Geophys. Res. 104, 18933–18956.
Weitz, C.M., Head, J.W., Pieters, C.M., 1998. Lunar and regional dark mantle deposits: geologic, multispectral, and modeling studies. J. Geophys. Res. 103, 22725–22759.
Wells, E., Hapke, B., 1977. Lunar soil: iron and titanium bands in the glass fraction. Science 195, 977–979.
Wetherill, G.W., 1988. Accumulation of Mercury from planetesimals. In: Vilas, F., Chapman, C.R., Matthews, M.S. (Eds.), Mercury. University of Arizona Press, Tuscon, Ariz., pp. 670–691.
Wetherill, G.W., 1994. Provenance of the terrestrial planets. Geochim. Comochim. Acta 58, 4513–4520.
Wilhelms, D.E., McCauley, J.F., 1971. Geologic map of the nearside of the Moon. Map I-703, Misc. Investigations Ser. U.S. Geological Survey, Denver, Colo.
Wilson, L., 1980. Relationships between pressures, volatile content and ejecta velocity in three types of volcanic eruptions. J. Volcanol. Geotherm. Res. 8, 297–313.
Wilson, L., Head, J.W., 1981. Ascent and eruption of basaltic magma on the Earth and Moon. J. Geophys. Res. 86, 2971–3001.
Wilson, L., Head, J.W., 2001. Lava fountains from the 1999 Tvashtar Catena fissure eruption on Io: implications for dike emplacement mechanisms, eruption rates, and crustal structure. J. Geophys. Res. 106, 32997–33004.
Wilson, L., Keil, K., 1997. The fate of pyroclasts produced in explosive eruptions on the asteroid 4 Vesta. Meteorit. Planet. Sci. 32, 813–823.
Zisk, S.H., Hodges, C.A., Moore, H.J., Shorthill, R.W., Thompson, T.W., Whitaker, E.A., Wilhelms, D.E., 1977. The Aristarchus–Harbinger region of the Moon: surface geology and history from recent remote sensing observations. Moon 17, 59–99.
Zurbuchen, T.H., Raines, J.M., Gloeckler, G., Krimigis, S.M., Slavin, J.A., Koehn, P.L., Killen, R.M., Sprague, A.L., McNutt Jr., R.L., Solomon, S.C., 2008. MESSENGER observations of the composition of Mercury's ionized exosphere and plasma environment. Science 321, 90–92.